Journal of Alloys and Compounds 695 (2017) 737–746

Contents lists available at ScienceDirect

Journal of Alloys and Compounds

journal homepage: http://www.elsevier.com/locate/jalcom

Incommensurately modulated structure and spectroscopic properties of $CaGd_2(MoO_4)_4$:Ho^{3+}/Yb^{3+} phosphors for up-conversion applications

Chang Sung Lim [a], Victor V. Atuchin [b, c, d, e, *], Aleksandr S. Aleksandrovsky [f, g], Maxim S. Molokeev [h, i], Aleksandr S. Oreshonkov [j, k]

[a] Department of Advanced Materials Science & Engineering, Hanseo University, Seosan 356-706, Republic of Korea
[b] Laboratory of Optical Materials and Structures, Institute of Semiconductor Physics, SB RAS, Novosibirsk 630090, Russia
[c] Functional Electronics Laboratory, Tomsk State University, Tomsk 634050, Russia
[d] Laboratory of Semiconductor and Dielectric Materials, Novosibirsk State University, Novosibirsk 630090, Russia
[e] Institute of Chemistry, Tyumen State University, Tyumen 525003, Russia
[f] Laboratory for Nonlinear Optics and Spectroscopy, Siberian Federal University, Krasnoyarsk 660041, Russia
[g] Laboratory of Coherent Optics, Kirensky Institute of Physics, SB RAS, Krasnoyarsk 660036, Russia
[h] Laboratory of Crystal Physics, Kirensky Institute of Physics, SB RAS, Krasnoyarsk 660036, Russia
[i] Department of Physics, Far Eastern State Transport University, Khabarovsk 680021, Russia
[j] Laboratory of Molecular Spectroscopy, Kirensky Institute of Physics, SB RAS, Krasnoyarsk 660036, Russia
[k] Department of Photonics and Laser Technologies, Siberian Federal University, Krasnoyarsk 660079, Russia

ARTICLE INFO

Article history:
Received 18 April 2016
Received in revised form
3 June 2016
Accepted 14 June 2016
Available online 16 June 2016

Keywords:
Molybdate
Sol-gel synthesis
Modulation
Upconversion
XRD
Raman

ABSTRACT

$CaGd_2(MoO_4)_4$:Ho^{3+}/Yb^{3+} phosphors doped by Ho^{3+} and Yb^{3+} (Ho^{3+} = 0 and 0.05, and Yb^{3+} = 0, 0.35, 0.40, 0.45 and 0.50) were successfully synthesized by the microwave sol-gel method. The synthesized particles, being formed after heat-treatment at 900 °C for 16 h, showed a well crystallized morphology. All compounds are (3 + 2)D incommensurately modulated with superspace group $I4_1/a(\alpha,\beta,0)00(-\beta,\alpha,0)00$. It was found that parameter $(\alpha^2 + \beta^2)^{1/2}$ is proportional to cell parameter *a* for all studied compositions and, therefore, modulation vector ***k*** is the same for all known $CaRE_2(MoO_4)_4$ compounds. The modulation vector invariance is a specific and valuable feature of this type of the structure. Under the excitation at 980 nm, the doped particles exhibited the yellow emission composed of green (545-nm) and red (655-nm) emission bands due to frequency upconversion (UC). The pump power dependence and CIE chromaticity of the UC emission were evaluated. The shape of UC bands in $CaGd_2(MoO_4)_4$:Ho^{3+}/Yb^{3+} is dependent on the Yb content due to the influence of the crystal field affecting a holmium ion. 13 Raman-active modes of the $CaGd_2(MoO_4)_4$ lattice were identified via a comparison of experimental Raman spectra and the lattice dynamics simulation results. Four additional Raman lines were found in the region of stretching vibrations and, at least, two additional modes are present in the bending mode region. These additional modes are ascribed to incommensurate crystal lattice modulation. Luminescence bands of Ho ions are severely broadened due to a statistical disorder in the $CaGd_{2-x}Yb_y(MoO_4)_4$ lattice.

1. Introduction

Rare earth bearing oxide crystals are the basic luminescent materials in modern photonics and laser technology because of high emission efficiency, thermal and chemical stability, and different spectroscopic properties that can be tuned by composition [1–9]. One of the most interesting effects observed in rare-earth-doped photoluminescence materials is the frequency conversion from near infrared radiation of low photon energy to visible high photon energy radiation or upconversion (UC) [10–20]. The UC materials have shown potential applications in various fields including noncontact and nondestructive temperature sensing,

* Corresponding author. Laboratory of Optical Materials and Structures, Institute of Semiconductor Physics, SB RAS, Novosibirsk 630090, Russia.
E-mail address: atuchin@isp.nsc.ru (V.V. Atuchin).

http://dx.doi.org/10.1016/j.jallcom.2016.06.134
0925-8388/

biomedical imaging and optical frequency conversion in photocatalytic composites [14,15,20–24].

The double alkaline earth lanthanide molybdates, $MRE_2(MoO_4)_4$ (M: alkaline-earth or bivalent rare-earth metal ion, RE: trivalent rare-earth or actinide ion), seem to be very promising host materials. Indeed, with a decrease of the alkaline-earth metal ion radii ($R_{Ca} < R_{Sr} < R_{Ba}$; R = ionic radius), the structure of $MB_2(MoO_4)_4$ could be transformed from the monoclinic structure to a highly disordered tetragonal scheelite-type structure [25]. As it was demonstrated for several crystals from this family, the disordered tetragonal-phase structure can accommodate doping RE^{3+} ions at high concentrations without structure disruption and defect generation that results in the excellent UC photoluminescence properties [18,25–32]. The incommensurate modulation was discovered in $CaEu_2(MoO_4)_4$ and $CaLa_2(MoO_4)_4$:Ho^{3+}/Yb^{3+} solid solutions [18,30,33], but the structure modulation characteristics of other molybdates $MB_2(MoO_4)_4$ remain unknown. In the present study, the $CaGd_2(MoO_4)_4$:Ho^{3+}/Yb^{3+} phosphors were synthesized by the microwave sol-gel method, and the crystal structure refinement, including modulation effects, as well as UC photoluminescence properties evaluation, were performed. Commonly, the Ho^{3+}/Yb^{3+} combination in a host is suitable for the infrared to visible light conversion through the UC process due to proper electronic energy level configurations of Ho^{3+} and Yb^{3+} ions, where the Ho^{3+} and Yb^{3+} ions are activator and sensitizer, respectively.

Earlier, the rare-earth-bearing molybdates were prepared by different technological routes, including solid-state reactions [26,28–30,32–37], co-precipitation [38–40], the sol-gel method [27], hydrothermal method [41,42], Pechini method [43,44] and the microwave-assisted hydrothermal method [45–47]. It is known that phosphor preparation by a solid-state method commonly requires high temperatures, long heating process and subsequent grinding, which may occasionally result in a particle surface damage. Comparatively, the sol-gel process possesses some advantages, including good particle homogeneity, low calcination temperature, small particle size and a narrow particle size distribution promising for good luminescent characteristics. The microwave synthesis has advantages as a very short reaction time, small-size particles, narrow particle size distribution and a high purity of the final polycrystalline products. Thus, the combined microwave sol-gel process is an optimal approach to the synthesis of high-quality luminescent materials for short time periods. In the present study, the $CaGd_{2-x}(MoO_4)_4$:Yb_y/Ho_z phosphors with the doping concentrations of Yb^{3+} and Ho^{3+} ($y = 0$, 0.35, 0.40, 0.45 and 0.50; $z = 0$, 0.05; $x = y + z$) were synthesized by the microwave sol-gel method, and the crystal structure refinement and UC photoluminescence properties evaluation were performed. To control the phase composition, the synthesized $CaGd_2(MoO_4)_4$:Ho^{3+}/Yb^{3+} particles were characterized by X-ray diffraction (XRD), scanning electron microscopy (SEM) and energy-dispersive X-ray spectroscopy (EDS). The pump power dependence and Commission Internationale de L'Eclairage (CIE) chromaticity of the UC emission intensity were evaluated in detail. The spectroscopic properties were examined comparatively using photoluminescence (PL) emission and Raman spectroscopy.

2. Experimental

Appropriate stoichiometric amounts of $Ca(NO_3)_2{\cdot}4H_2O$ (99%, Sigma-Aldrich, USA), $Gd(NO_3)_3{\cdot}6H_2O$ (99%, Sigma-Aldrich, USA), $(NH_4)_6Mo_7O_{24}{\cdot}4H_2O$ (99%, Alfa Aesar, USA), $Ho(NO_3)_3{\cdot}5H_2O$ (99.9%, Sigma-Aldrich, USA), $Yb(NO_3)_3{\cdot}5H_2O$ (99.9%, Sigma-Aldrich, USA), citric acid (99.5%, Daejung Chemicals, Korea), NH_4OH (A.R.), ethylene glycol (A.R.) and distilled water were used as initial reagents to prepare the $CaGd_{2-x}(MoO_4)_4$:Yb_y/Ho_z ($y = 0$, 0.35, 0.40, 0.45 and 0.50; $z = 0$, 0.05; $x = y + z$) compositions. The chemical compositions and sample notations of $CaGd_{2-x}(MoO_4)_4$:Yb^{3+}/Ho^{3+} ($x = Yb^{3+} + Ho^{3+}$) are shows in Table 1. To prepare pure $CaGd_2(MoO_4)_4$, 0.4 mol% $Ca(NO_3)_2{\cdot}4H_2O$ and 0.229 mol% $(NH_4)_6Mo_7O_{24}{\cdot}4H_2O$ were dissolved in 20 mL of ethylene glycol and 80 mL of 5 M NH_4OH under vigorous stirring and heating. Subsequently, 0.8 mol% $Gd(NO_3)_3{\cdot}6H_2O$ and citric acid (with a molar ratio of citric acid to total metal ions of 2:1) were dissolved in 100 mL of distilled water under vigorous stirring and heating. Then, the solutions were mixed in 400 mL Pyrex glass under vigorous stirring and heating at 80–100 °C. At the end, highly transparent solutions were obtained and adjusted to pH = 7–8 by the addition of NH_4OH or citric acid. To prepare $CaGd_{1.6}(MoO_4)_4$:$Yb_{0.35}$/$Ho_{0.05}$, the mixture of 0.64 mol% $Gd(NO_3)_3{\cdot}6H_2O$, 0.14 mol% $Yb(NO_3)_3{\cdot}5H_2O$ and 0.02 mol% $Ho(NO_3)_3{\cdot}5H_2O$ was used for the creation of the rare-earth-carrying solution. To prepare $CaGd_{1.55}(MoO_4)_4$:$Yb_{0.40}$/$Ho_{0.05}$, the mixture of 0.62 mol% $Gd(NO_3)_3{\cdot}6H_2O$, 0.16 mol% $Yb(NO_3)_3{\cdot}5H_2O$ and 0.02 mol% $Ho(NO_3)_3{\cdot}5H_2O$ was employed for the creation of the rare-earth-carrying solution. To prepare $CaGd_{1.50}(MoO_4)_4$:$Yb_{0.45}$/$Ho_{0.05}$, the mixture of 0.6 mol% $Gd(NO_3)_3{\cdot}6H_2O$, 0.18 mol% $Yb(NO_3)_3{\cdot}5H_2O$ and 0.02 mol% $Ho(NO_3)_3{\cdot}5H_2O$ was used for the creation of the rare-earth-carrying solution. To prepare $CaGd_{1.45}(MoO_4)_4$:$Yb_{0.50}$/$Ho_{0.05}$, the rare-earth-containing solution was generated using 0.58 mol% $Gd(NO_3)_3{\cdot}6H_2O$, 0.2 mol% $Yb(NO_3)_3{\cdot}5H_2O$ and 0.02 mol% $Ho(NO_3)_3{\cdot}5H_2O$.

The transparent solutions after vigorous stirring and heating until the deduced volume of 200 mL was reached in 400 mL Pyrex glass were placed into a microwave oven operating at the frequency of 2.45 GHz and the maximum output power of 1250 W for 30 min. The microwave reaction working cycle was controlled very precisely between 40 s on and 20 s off for 15 min followed by a further treatment of 30 s on and 30 s off for 15 min. Water and ethylene glycol were evaporated slowly at their boiling points. Ethylene glycol is a polar solvent with the boiling point of 197 °C, and this solvent is a good medium for the microwave process. Respectively, if ethylene glycol is used as a solvent, the reactions proceed at the boiling point temperature. When microwave radiation is supplied to the ethylene-glycol-based solution, the components dissolved in the ethylene glycol can couple. The charged particles vibrate in the electric field interdependently when a large amount of microwave radiation is supplied to ethylene glycol. After microwave process, each sample of 30 mL was being treated with ultrasonic radiation for 10 min to produce a light yellow transparent sol. After this stage, the light yellow sols were dried at 120 °C in a dry oven to obtain black dried gels. The black dried gels were being ground and preheat-treated enough at 350 °C for 12 h to evaporate the remaining ethylene glycol and synthesized continuously in an individually distributed state due to the evaporated ethylene glycol at 900 °C for 16 h in the air with a 100 °C interval between 600 and 900 °C. Finally, the white and pink particles were obtained for pure $CaGd_2(MoO_4)_4$ and the doped compositions, respectively.

The powder diffraction data of the synthesized particles for Rietveld analysis were collected over the range of $2\theta = 5$–$110°$ at room temperature with a D/MAX 2200 (Rigaku, Japan) diffractometer (Cu-Kα radiation, θ-2θ geometry). The step size of 2θ was 0.02°, and the counting time was 5 s per step. The microstructure and surface morphology were observed using SEM/EDS (JSM-5600, JEOL, Japan). The PL spectra were recorded using a spectrophotometer (Perkin Elmer LS55, UK) at room temperature. Raman spectra measurements were performed using a LabRam Aramis (Horiba Jobin-Yvon, France) with the spectral resolution of 2 cm^{-1}. The 514.5-nm line of an Ar ion laser was used as an excitation source; to avoid sample decomposition, the samples were exposed to a power level that was maintained at 0.5 mW.

3. Results and discussion

The XRD patterns recorded from the synthesized molybdates are shown in Fig. 1 and Figs. 1S–5S. In general, the patterns of solid solutions $CaGd_{2-x}(MoO_4)_4$:Yb_y/Ho_z ($y = 0, 0.35, 0.40, 0.45$ and 0.50; $z = 0, 0.05$) are similar. The difference profile plot of $CaGd_2(MoO_4)_4$ is shown in Fig. 1. The difference profile plots of $CaGd_2(MoO_4)_4$:Yb_y/Ho_z are very similar to that of $CaGd_2(MoO_4)_4$ and they are not shown. Earlier, it was obtained that, within the $CaGd_{2(1-x)}Eu_{2x}(MoO_4)_4$ series, all compounds are (3 + 2)D incommensurately modulated with superspace group $I4_1/a(\alpha,\beta,0)$ $00(-\beta,\alpha,0)00$ and parameters α and β were determined for $CaEu_2(MoO_4)_4$ [30,33]. The crystals under investigation are related to this family and, first of all, the Le Bail decomposition was applied using the JANA2006 software [48]. The refinements were stable and gave low R-factors, as shown in Table 2. All peaks in each pattern were accounted by one phase in superstructure space group $I4_1/a(\alpha,\beta,0)00(-\beta,\alpha,0)00$ that proves high purity of all samples.

It is known that the wavevector of incommensurate modulation $\boldsymbol{k}$ in a reciprocal space can be expressed with the help of fractional components α, β, γ and three reciprocal lattice vectors $\boldsymbol{a}^*$, $\boldsymbol{b}^*$ and $\boldsymbol{c}^*$: $\boldsymbol{k} = \alpha\boldsymbol{a}^* + \beta\boldsymbol{b}^* + \gamma\boldsymbol{c}^*$ [49,50]. In our case for the tetragonal crystal, the relations $|\boldsymbol{a}^*| = |\boldsymbol{b}^*| = 1/a$, where a – cell parameter, and $|\boldsymbol{k}| = |\alpha\boldsymbol{a}^* + \beta\boldsymbol{b}^*| = (\alpha^2 + \beta^2)^{1/2}|\boldsymbol{a}^*| = (\alpha^2 + \beta^2)^{1/2}/a$ are valid. From the curve shown in Fig. 2, relation $|\boldsymbol{k}| = |(\alpha^2 + \beta^2)^{1/2}/a = \text{const}$ is evident. Thus, it can be reasonably concluded that modulation vector $\boldsymbol{k}$ is the same for all $CaRE_2(MoO_4)_4$ compounds independently from RE selection. Supposedly, this rule can be generalized for different M^{2+} ions in $MRE_2(MoO_4)_4$, which structure features are unknown up to now [26,27,29,31,32,51].

To consider the modulation mechanism in the molybdate crystals, let us imagine the system of four 1D node chains with the following periods: 1) $a = 12/12$ Å = 1 Å; 2) $a = 12/11$ Å ≈ 1.091 Å; 3) $a = 12/10$ Å = 1.2 Å; 4) $a = 12/9$ Å ≈ 1.333 Å. The chain period increases with a chain number. It can be supposed that the chains are modulated with vector $|\boldsymbol{k}| = 0.25$ Å^{-1}. The value is the same for all the chains similar to the case of $CaGd_2(MoO_4)_4$:Yb_y/Ho_z crystals. Then, relation $\alpha = |\boldsymbol{k}||\boldsymbol{a}|$ is valid because $\boldsymbol{k} = \frac{\alpha}{\boldsymbol{a}}$. In this case, for the node chains, there is 1) $\alpha = 1$ Å × 0.25 Å^{-1} = 0.25 = 1/4 = 3/12; 2) $\alpha = 12/11$ Å × 0.25 Å^{-1} = 3/11; 3) $\alpha = 12/10$ Å × 0.25 Å^{-1} = 3/10; 4) $\alpha = 12/9$ Å × 0.25 Å^{-1} = 3/9. Thus, three vectors $\boldsymbol{k}^{-1}$ with magnitude $|\boldsymbol{k}^{-1}| = 4$Å are equal to 12, 11, 10 and 9 periods of chains 1, 2, 3 and 4, respectively. Visually, it can be imagined as shown in Fig. 3, where the nodes of all chains are modulated by color from white to black. Each color gradation can be considered as a characteristic of the node related to a shift or atom settlement. From Fig. 3, it is evident that, if we take the node with a definite number being the same for all chains, the state (color) of the node is strongly different from chain to chain. Alternatively, if one considers the nodes positioned at a definite and equal distance from the first node of each chain, the state (color) of the nodes is the same. This effect appeared due to the persistent modulation vector which is independent from the cell dimension.

Earlier, in Ref. 30, it was stated that incommensurately modulated structures in $MRE_2(MoO_4)_4$ compounds are generated by ordering the M cations and vacancies. Then, in accordance with the results of Ref. 30 and the present study, the distance between M-cations and vacancies is independent from ionic radii and, respectively, from the unit cell parameters of crystals $MRE_2(MoO_4)_4$. However, the distribution of M-cations/vacancies over the lattice nodes will be different in different $MRE_2(MoO_4)_4$ molybdates. The modulation vector invariance is a specific and valuable feature of this type of the structure. The distance-dependent Coulomb interaction seems to be the source of the vacancy/cation distribution in reference to distance instead of reference to angles. The energy minimum related to the structure stabilization is reached at the characteristic distances between the vacancy/cations. The distances may be not equal to cell parameters and, then, the incommensurate modulation appears. Thus, the dependence shown in Fig. 2 opens a possibility to predict the parameter $(\alpha^2 + \beta^2)^{1/2}$ in other, presently unstudied, $MRE_2(MoO_4)_4$ molybdates.

As far as the calculation of Raman spectra from a modulated crystal structure is much more time-consuming, we have found and refined an averaged crystal structure without modulation of all compounds under investigation. Rietveld refinement was performed using TOPAS 4.2 [52]. All peaks of the compounds were indexed by tetragonal cell ($I4_1/a$) with parameters close to $CaGd_2(MoO_4)_4$ [25] and this crystal structure was taken as starting point for the Rietveld refinement. The Ca/Gd site was occupied by Ca/Gd/Yb/Ho ions (Fig. 4) with fixed occupancies according to nominal chemical formulas. Therefore, in the compounds. there are one Ca/Gd/Yb/Ho site with Wyckoff position 4b, one Mo site (4a) and one O site (16f), as shown in Fig. 4. As far as only O ion is in general position, only its three coordinates were refined. Thermal parameters of all ions were refined isotropically. The refinements were stable and gave low R-factors (Table 3, Figs. 1S–5S). The atom coordinates and main bond lengths are depicted in Tables 2S and 3S, respectively. The trend of the cell volume increase per averaged ionic radii of Gd/Yb/Ho atoms, as shown in Fig. 5, proves the suggested general chemical formula of $CaGd_{2-x}(MoO_4)_4$:Yb_y/Ho_z solid solutions. Obviously, the cell parameters are almost independent when average IR is lower than 1.04 and, then, increase abruptly when average IR increases.

The SEM image of the synthesized $CaGd_2(MoO_4)_4$ particles is shown in Fig. 6. The particle morphology of other samples is similar (not shown) to that of $CaGd_2(MoO_4)_4$. From Fig. 6, it is seen that the as-synthesized sample contain particles with a fine and homogeneous morphology and the characteristic particle size is 2–5 μm. The particles are partly coalesced into agglomerates and this is induced by interdiffusions among the grains at 600–900 °C. Previously, similar morphology was demonstrated for different oxide products, including molybdates, formed by solid state reaction at appropriate temperatures [20,27,31,34,47,53,54]. Thus, the coalescent particle morphology may be considered as an universal indicator of high chemical homogeneity and structural quality of powder products. The recorded EDS patterns and quantitative compositions of the synthesized (a) $CaGd_{1.6}(MoO_4)_4$:$Yb_{0.35}$/$Ho_{00.5}$ and (b) $CaGd_{1.5}(MoO_4)_4$:$Yb_{0.45}$/$Ho_{0.05}$ samples are shown in Fig. 6S. Only constituent elements are found in the samples and the quantitative compositions are in good relation to nominal ones. This result confirms that the designed chemical composition is persistent during the cyclic microwave-modified sol-gel synthesis. It must be emphasized that the microwave sol-gel process provides the energy uniformly to the bulk of the material so that the fine particles with controlled morphology can be fabricated for a short time. Besides, the method is a cost-effective way to provide homogeneous double molybdate products with an easy scale-up potential, and it is a viable alternative for the rapid synthesis of UC particles. The post heat-treatment at 900 °C in the air plays an important role in the pure phase formation, well-defined

Table 1
Chemical compositions and sample notations of $CaGd_{2-x}(MoO_4)_4$:yYb^{3+}/zHo^{3+} ($x = Yb^{3+} + Ho^{3+}$).

Sample	Yb^{3+} (y)	Ho^{3+} (z)	$x = Yb^{3+} + Ho^{3+}$	Yb^{3+}/Ho^{3+}
$CaGd_{1.60}(MoO_4)_4$:yYb/zHo	0.35	0.04	0.40	7:1
$CaGd_{1.55}(MoO_4)_4$: yYb/zHo	0.40	0.03	0.45	8:1
$CaGd_{1.50}(MoO_4)_4$: yYb/zHo	0.45	0.02	0.50	9:1
$CaGd_{1.45}(MoO_4)_4$: yYb/zHo	0.50	0.01	0.55	10:1

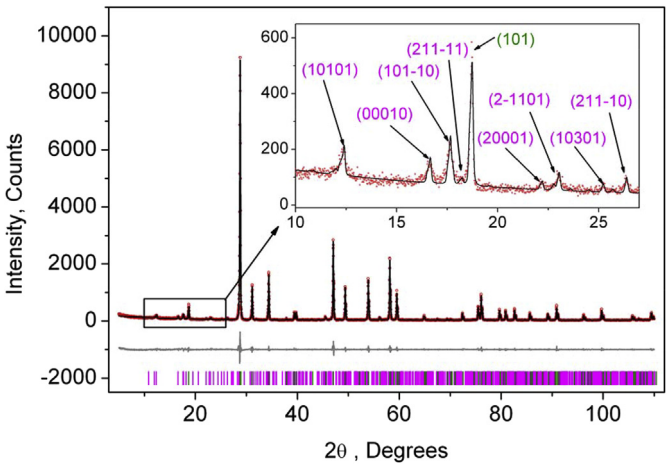

Fig. 1. The difference profile plot of $CaGd_2(MoO_4)_4$. Red dots - experimental pattern (Y_{obs}), black line – calculated pattern (Y_{calc}), grey line - difference (Y_{obs}–Y_{calc}), green sticks – main Bragg peaks, purple – modulated peaks. A zoomed part of the difference plot at low angles is shown in the insert, and the reflection indices in notation (3 + 2)D are shown with numbers in brackets. (For interpretation of the references to colour in this figure legend, the reader is referred to the web version of this article.)

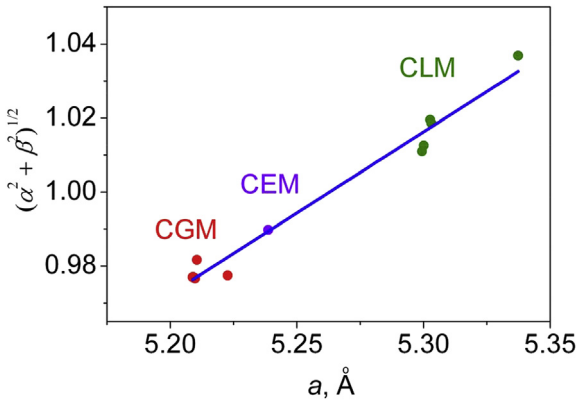

Fig. 2. The modulation parameters dependence on the *a* cell parameter in the $MRE_2(MoO_4)_4$ molybdates. The compounds $CaGd_2(MoO_4)_4$:Yb_y/Ho_z (CGM) (present study), $CaEu_2(MoO_4)_4$ (CEM) [33] and $CaLa_2(MoO_4)_4$ (CLM) [18] are shown.

microparticle morphology and oxygen deficiency compensation.

The Raman spectra recorded from $CaGd_2(MoO_4)_4$:Ho^{3+}/Yb^{3+} are shown in Fig. 7. The vibrational representation for the tetragonal phase at Brillouin zone center for $CaGd_2(MoO_4)_4$ averaged structure is:

$$\Gamma_{vibr} = 3A_g + 6B_g + 6E_g + 6A_u + 3B_u + 6E_u,$$

The Raman and infrared active modes are $\Gamma_{raman} = 3A_g + 6B_g + 6E_g$ and $\Gamma_{infrared} = 5A_u + 5E_u$, correspondingly. The vibrational representation for the tetragonal phase at the Brillouin zone center for all rare-earth doped average structures is:

$$\Gamma_{vibr} = 3A_g + 8B_g + 8E_g + 8A_u + 3B_u + 8E_u$$

The Raman and infrared active modes are $\Gamma_{raman} = 3A_g + 8B_g + 8E_g$ and $\Gamma_{infrared} = 7A_u + 7E_u$, correspondingly.

Comparison of lattice dynamics simulation for $CaGd_2(MoO_4)_4$ and $CaGd_2(MoO_4)_4$:Ho^{3+}/Yb^{3+} averaged crystal structures shows that the difference between $CaGd_2(MoO_4)_4$ and $CaGd_2(MoO_4)_4$:Ho^{3+}/Yb^{3+} Raman spectra should be observed in the region below 100 cm^{-1}, no noticeable changes in other parts of the spectra should appear regardless of the rare-earth ion concentration. As can be seen from Fig. 7, the number of lines and shape of the observed Raman spectra in the region of 270–450 cm^{-1} are almost identical for all samples of both $CaGd_2(MoO_4)_4$ and $CaGd_2(MoO_4)_4$:Ho^{3+}/Yb^{3+}. The bands corresponding to the ν_2 and ν_4 bending modes of the MoO_4 groups are dominant in this wavenumber range. Two spectral lines in the vicinity of 400 cm^{-1} correspond to asymmetric bending modes ν_4 of MoO_4, and two strong peaks in the range of 300–370 cm^{-1} are symmetric bending modes ν_2. However, for a more precise deconvolution of Raman bands in this area, we should add two additional lines at 320 and 350 cm^{-1}. According to the lattice dynamics simulation, a Raman spectrum above 700 cm^{-1} should contain only three active Raman lines: symmetric stretching mode (A_{1g} symmetry) ν_1, and antisymmetric stretching modes ν_3 (B_g and E_g symmetry) for $CaGd_2(MoO_4)_4$ and all $CaGd_2(MoO_4)_4$:Ho^{3+}/Yb^{3+}. Taking into account that, with the exception of incommensurate modulation effects, almost all XRD peaks were indexed by a tetragonal unit cell (space group $I4_1/a$) with the parameters close to the $CaMoO_4$ scheelite-type structure, the number of Raman-active lines and their intensities distribution for scheelite-type structure compounds [55], $CaMoO_4$ [56,57] and $CaGd_2(MoO_4)_4$ in the range above 700 cm^{-1} should be the same. In our measurements, however, the Raman spectrum of $CaGd_2(MoO_4)_4$ contains additional lines in this range, as evident from Fig. 7. The comparison of Raman modes observed in $CaGd_2(MoO_4)_4$ with the modes earlier found in scheelite-type structure compounds is presented in Table 4.

The presence of additional lines in the regions of stretching and bending vibrational modes of MoO_4 can be described as tetrahedron disordering [58]. However, no indications of the tetrahedron disorder were found by XRD analysis. Thus, we can conclude that

Table 2
Main parameters and processing of Le Bail fitting of the $CaGd_2(MoO_4)_4$:*x*Yb,*y*Ho samples by using (3 + 1)D modulation.

Compound	$CaGd_2(MoO_4)_4$	$CaGd_{1.6}(MoO_4)_4$:0.35Yb,0.05Ho	$CaGd_{1.55}(MoO_4)_4$:0.4Yb,0.05Ho	$CaGd_{1.5}(MoO_4)_4$:0.45Yb,0.05Ho	$CaGd_{1.45}(MoO_4)_4$:0.5Yb,0.05Ho
Sp.Gr.	$I4_1/a(\alpha,\beta,0)00$ $(-\beta,\alpha,0)00$	$I4_1/a(\alpha,\beta,0)00$ $(-\beta,\alpha,0)00$	$I4_1/a(\alpha,\beta,0)00$ $(-\beta,\alpha,0)00$	$I4_1/a(\alpha,\beta,0)00$ $(-\beta,\alpha,0)00$	$I4_1/a(\alpha,\beta,0)00$ $(-\beta,\alpha,0)00$
q-vector	[0.53756(9), 0.81639(7), 0]	[0.5361(1), 0.81642(8), 0]	[0.5363(1), 0.81664(9), 0]	[0.5361(1), 0.81666(8), 0]	[0.5409(1), 0.8192(1), 0]
a, Å	5.22267(5)	5.20976(6)	5.20882(6)	5.20901(6)	5.32059(6)
c, Å	11.5056(2)	11.4660(2)	11.4619(2)	11.4640(2)	11.4687(2)
V, Å^3	313.830(6)	311.207(7)	310.982(7)	311.062(8)	311.367(8)
2θ-range, °	5–110	5–110	5–110	5–110	5–110
R_{wp}, %	12.90	13.93	13.62	13.50	13.10
R_p, %	9.26	10.21	9.87	9.65	9.14
R_{exp}, %	9.99	11.30	11.16	10.24	9.80
χ^2	1.29	1.23	1.22	1.32	1.34

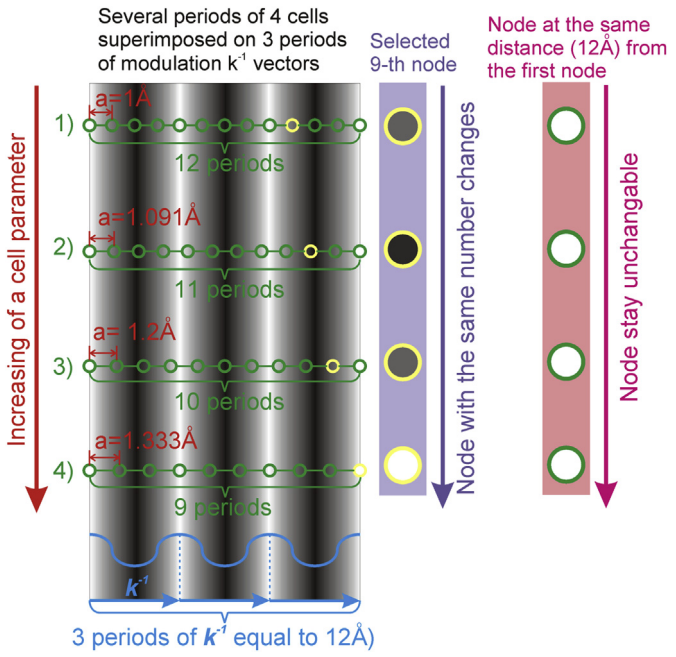

Fig. 3. Four chains with a period increasing from 1 to 1.333 Å, where nodes and/or atoms are depicted with circles. The modulation with the period of $|k|^{-1} = 4$ Å is superimposed as a grey field with the intensity variation. The circle brightness indicates the node state. The ninth circle of each chain is depicted by yellow color for the clarity of comparison. (For interpretation of the references to colour in this figure legend, the reader is referred to the web version of this article.)

the appearance of additional Raman bands is connected with incommensurate modulation within the $CaGd_2(MoO_4)_4$ crystal structure [51]. Above 700 cm^{-1}, the spectra of undoped $CaGd_2(MoO_4)_4$, from one side, and those of the samples doped with Ho and Yb, from other side, are markedly different. A more detailed analysis of doped samples' emission will be presented below. However, the active line corresponding to the full symmetric stretching of MoO_4 tetrahedron is still dominating in all recorded spectra.

The UC photoluminescence emission spectra of the as-prepared (a) $CaGd_{1.6}(MoO_4)_4:Yb_{0.35}/Ho_{0.05}$, (b) $CaGd_{1.55}(MoO_4)_4:Yb_{0.40}/Ho_{0.05}$, (c) $CaGd_{1.5}(MoO_4)_4:Yb_{0.45}/Ho_{0.05}$, and (d) $CaGd_{1.45}(MoO_4)_4:Yb_{0.50}/Ho_{0.05}$ particles excited by 980 nm at 24 °C are shown in Fig. 8. The samples exhibited yellow emissions based on the combination of strong emission bands at 545 and 655 nm in green and red spectral regions, respectively. The strong 545 nm

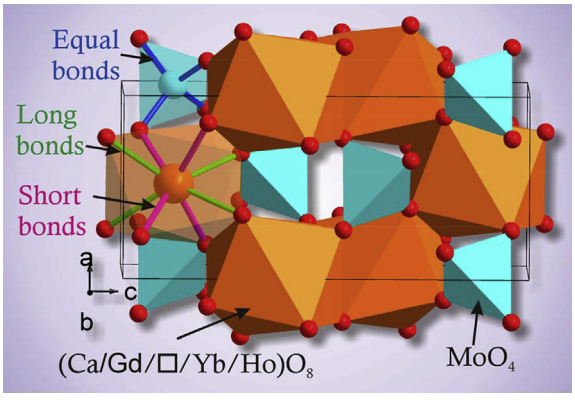

Fig. 4. The averaged crystal structure of $CaGd_{2-x}(MoO_4)_4:y$Yb,zHo crystals in space group $I4_1/a$. The unit cell is outlined.

emission band in the green region corresponds to the $^5S_2/^5F_4 \rightarrow {}^5I_8$ transition in Ho^{3+} ions, while the strong emission 655 nm band in the red region appears due to the $^5F_5 \rightarrow {}^5I_8$ transition in Ho^{3+} ions. The Ho^{3+} ion activator is the luminescence center for these UC particles, and the Yb^{3+} ions, as a sensitizer, enhances the UC luminescence efficiency. As it is evident from Fig. 8, the UC intensity is dependent on the Yb^{3+}:Ho^{3+} ratio in samples (a) 7:1, (b) 8:1, (c) 9:1 and (d) 10:1. When the Yb^{3+}:Ho^{3+} ratio is 9:1, the UC intensity of (c) $CaGd_{1.5}(MoO_4)_4:Yb_{0.45}/Ho_{0.05}$ particles is the highest in the red emission of the $^5F_5 \rightarrow {}^5I_8$ transition, while (d) $CaGd_{1.45}(MoO_4)_4:Yb_{0.50}/Ho_{0.05}$ particles shows the highest in the green emission of the $^5S_2/^5F_4 \rightarrow {}^5I_8$ transition, because of the different role of the Yb^{3+}:Ho^{3+} ratio for the $^5F_5 \rightarrow {}^5I_8$ transition and the $^5S_2/^5F_4 \rightarrow {}^5I_8$ transition. On the same feature, the Yb^{3+}:Ho^{3+} ratios are 9:1 and 10:1, in the case of the UC intensity of $CaLa_{1.5}(MoO_4)_4:Yb_{0.45}/Ho_{0.05}$ and $CaLa_{1.45}(MoO_4)_4:Yb_{0.50}/Ho_{0.05}$ particles is also the highest for different bands [18].

The logarithmic scale dependence of the UC emission intensities at 545 and 655 nm on the working pump power over the range from 20 to 110 mW in the $CaGd_{1.55}(MoO_4)_4:Yb_{0.45}/Ho_{0.05}$ sample is shown in Fig. 9. In an ideal UC process, UC emission intensity I is proportional to the slope value n of the irradiation pumping power P, where n is the number of pumping photons required to produce UC emission or, in another words, to excite the upper emitting energy level [59]:

$$I \propto P^n$$

$$\mathrm{Ln}I \propto n\mathrm{Ln}P\,.$$

The experimental dependencies in Fig. 9 show the slopes of $n = 1.72$ and 1.86 for green emission at 545 nm and red emission at 655 nm, respectively. This result provides that the UC mechanism of the green and red emissions can be explained by a two-photon UC process in Ho^{3+}/Yb^{3+} co-doped phosphors.

Based on the results of pump power dependence, the known schematic energy level diagrams of Ho^{3+} (activator) and Yb^{3+} (sensitizer) ions in the as-prepared $CaGd_{2-x}(MoO_4)_4:Yb_y/Ho_z$ samples and the UC mechanisms, accounting for the green and red emissions during 980 nm laser excitation, are depicted in Fig. 10. The UC emissions are generated by the two-photon process of energy transfer (ET) and excited state absorption (ESA). Initially, the Yb^{3+} ion sensitizer is excited from the $^2F_{7/2}$ level to the $^2F_{5/2}$ level under excitation by 980 nm light; the Yb^{3+} ion sensitizer transfers its energy to the Ho^{3+} ions. Then, the Ho^{3+} ions are populated from the $^5I_8$ ground state to the $^5I_6$ excited state. This is a phonon-assisted energy transfer process because of the energy mismatch between the $^2F_{5/2}$ level of Yb^{3+} and the $^5I_6$ level of Ho^{3+}. Then, the Ho^{3+} in the $^5I_6$ level is excited to the $^5S_2$ or $^5F_4$ levels by the next energy transfer from Yb^{3+}. In addition, the $^5S_2/^5F_4$ level of Ho^{3+} can be populated through the excited state absorption. Finally, the green emission at around 545 nm, corresponding to the $^5S_2/^5F_4 \rightarrow {}^5I_8$ transition, takes place. For the red emission, the population of the $^5F_5$ level can be created by two different channels. One channel is the nonradiative relaxation of Ho^{3+} from the $^5S_2/^5F_4$ level to the $^5F_5$ level. The other channel is closely related to the $^5I_7$ level populated by non-radiative relaxation from the $^5I_6$ excited state. The Ho^{3+} in the $^5I_7$ level is excited to the $^5F_5$ level by the energy transfer from Yb^{3+} and, then, relaxes to the $^5F_5$ level. Therefore, the red emission around 655 nm corresponds to the $^5F_5 \rightarrow {}^5I_8$ transition.

The CIE chromaticity diagram showing the color coordinates of the $CaGd_{2-x}(MoO_4)_4:Yb_y/Ho_z$ phosphors is shown in Fig. 11. Here, the points related to emission from the samples with compositions (a) $CaGd_{1.6}(MoO_4)_4:Yb_{0.35}/Ho_{0.05}$, (b) $CaGd_{1.55}(MoO_4)_4:Yb_{0.40}/$

Table 3
Main parameters of processing and Rietveld refinement the $CaGd_2(MoO_4)_4$:*x*Yb,*y*Ho samples by using average crystal structure.

Compound	$CaGd_2(MoO_4)_4$	$CaGd_{1.6}(MoO_4)_4$:0.35Yb,0.05Ho	$CaGd_{1.55}(MoO_4)_4$:0.4Yb,0.05Ho	$CaGd_{1.5}(MoO_4)_4$:0.45Yb,0.05Ho	$CaGd_{1.45}(MoO_4)_4$:0.5Yb,0.05Ho
Sp.Gr.	$I4_1/a$	$I4_1/a$	$I4_1/a$	$I4_1/a$	$I4_1/a$
a, Å	5.22070(7)	5.20931(6)	5.20879(7)	5.20846(8)	5.20865(9)
c, Å	11.5027(2)	11.4683(2)	11.4652(2)	11.4661(1)	11.4653(3)
V, Å^3	313.51(1)	311.215(9)	311.07(1)	311.05(1)	311.05(1)
2θ-range, °	5–110	5–110	5–110	5–110	5–110
No. of reflections	104	104	104	104	104
No. of refined parameters	7	7	7	7	7
R_{wp}, %	14.71	16.54	17.08	17.41	18.56
R_p, %	9.84	11.55	12.01	11.76	12.12
R_{exp}, %	9.97	11.28	11.14	10.22	9.79
χ^2	1.48	1.47	1.53	1.70	1.90
R < *SUB* > *B* < /*SUB*>, %	1.18	2.90	2.83	2.49	1.78

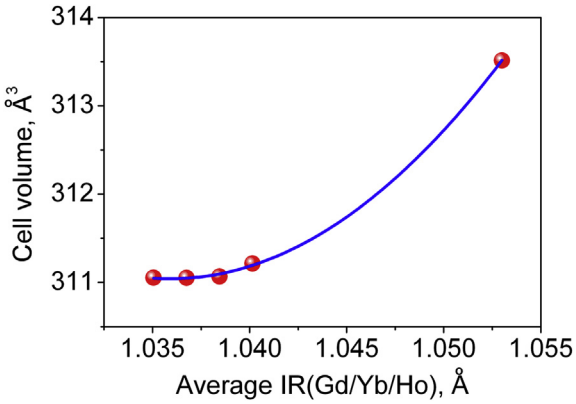

Fig. 5. The unit cell volume dependence on the averaged ionic radii of rare earth cations in $CaGd_{2-x}(MoO_4)_4$:*y*Yb,*z*Ho crystals.

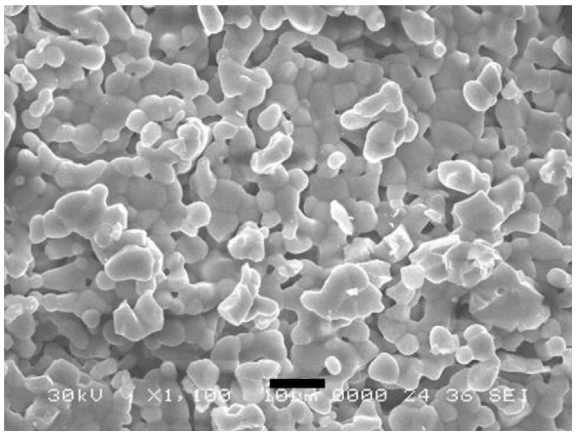

Fig. 6. A scanning electron microscopy image of the synthesized $CaGd_2(MoO_4)_4$ particles.

$Ho_{0.05}$, (c) $CaGd_{1.5}(MoO_4)_4$:$Yb_{0.45}$/$Ho_{0.05}$, and (d) $CaGd_{1.45}(MoO_4)_4$:$Yb_{0.50}$/$Ho_{0.05}$ are inserted. The yellow emission color coordinates of the samples are well matched with the standard equal energy point. This result indicates the attractive yellow UC emissions acceptable for the potential active components in new optoelectronic devices and luminescent devices.

The shape of UC bands in $CaGd_2(MoO_4)_4$ is found to be dependent on the Yb ions content, as can be seen in more detail in Figs. 7S and 8S. For the luminescence from $^5S_2/^5F_4$, the manifold variation of the band shape becomes well-pronounced only at the highest Yb

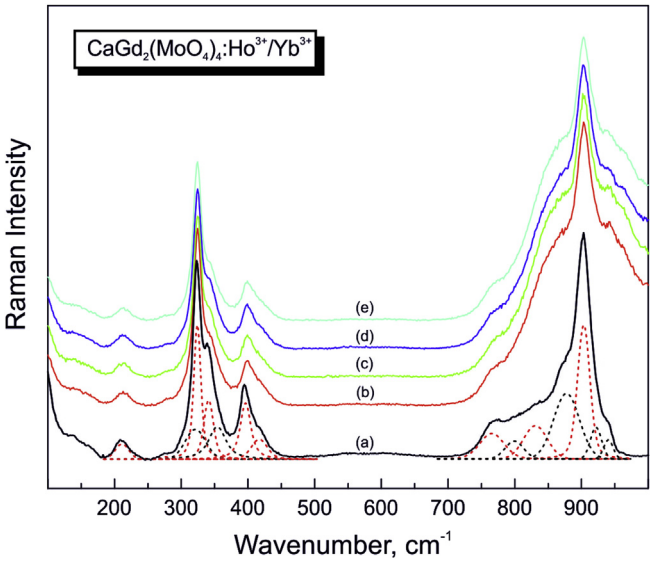

Fig. 7. The Raman spectra of $CaGd_2(MoO_4)_4$:*x*Yb,*y*Ho: (a) – undoped, (b) – 0.35Yb,0.05Ho, (c) – 0.4Yb,0.05Ho, (d) – 0.45Yb,0.05Ho, (e) – 0.5Yb,0.05Ho.

content, while, for the luminescence from $^5F_5$ manifold, severe variation is observable even at the Yb content equal to 0.45. In case of previously studied $CaLa_2(MoO_4)_4$:Ho,Yb, the band shape variation on the Yb content was not detected. The presence of this effect in $CaGd_2(MoO_4)_4$:Ho,Yb might be ascribed to the incommensurate modulation within the $CaGd_2(MoO_4)_4$ crystal structure; however, this suggestion must be ruled out since similar modulation in $CaLa_2(MoO_4)_4$ is expected to give a similar influence. Therefore, this effect, evidently, is due to the influence of the crystal field on the Ho ion. The Gd ion radius and, especially, the Yb ion radius are smaller than that of the La ion, and that leads to a closer position of the ligands surrounding the Ho dopant ion in the substituting Gd (or Yb) ion in the $CaGd_2(MoO_4)_4$ lattice than that in a $CaLa_2(MoO_4)_4$ one. This difference is very modest, but, due to a strong dependence of the crystal field on the distance, it leads to band shape variation in the case of $CaGd_2(MoO_4)_4$.

The emission spectra of the Ho,Yb-codoped samples of $CaGd_{1.6}(MoO_4)_4$:$Yb_{0.35}$/$Ho_{0.05}$, $CaGd_{1.55}(MoO_4)_4$:$Yb_{0.40}$/$Ho_{0.05}$, $CaGd_{1.5}(MoO_4)_4$:$Yb_{0.45}$/$Ho_{0.05}$, and $CaGd_{1.45}(MoO_4)_4$:$Yb_{0.50}$/$Ho_{0.05}$ are shown in Fig. 12. The excitation wavelength and power on the sample were 514.5-nm (Ar ion laser) and 0.5 mW, respectively. The emission spectrum of the pure $CaGd_2(MoO_4)_4$ sample contains predominantly the intense Raman lines analyzed above within this article. However, the shape of the emission spectra recorded from

Table 4
Analysis of Raman spectra of $CaGd_2(MoO_4)_4$ and related compounds.

Symmetry type	Observed Raman modes, cm^{-1}			
	[55]	[56]	[57]	$CaGd_2(MoO_4)_4$ (exp)
				939.6[a]
				921.4[a]
A_g	871	877	877	903.4
				880.8[a]
B_g	771	845.5	845	830.8
				801.2[a]
E_g	748	792	792	770.3
E_g	354	402.5	402	415
B_g	350	391	391	395
B_g	323	327.5	328	352[a]
				340
A_g	323	321.5	322	323
				320[a]
E_g	193	267		275
B_g	171	214		211
A_g	107	204.5	205	
E_g	78	189.5	143	
E_g	71	143	112	
B_g	65	111.5	86	

[a] Additional lines arising from spectra deconvolution but absent in lattice dynamics simulation.

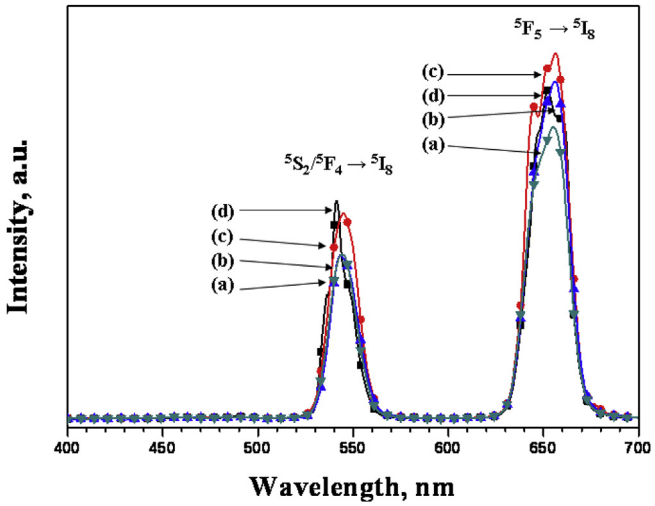

Fig. 8. The upconversion photoluminescence emission spectra of (a) $CaGd_{1.6}(MoO_4)_4$:$Yb_{0.35}$/$Ho_{0.05}$, (b) $CaGd_{1.55}(MoO_4)_4$:$Yb_{0.40}$/$Ho_{0.05}$, (c) $CaGd_{1.5}(MoO_4)_4$:$Yb_{0.45}$/$Ho_{0.05}$ and (d) $CaGd_{1.45}(MoO_4)_4$:$Yb_{0.50}$/$Ho_{0.05}$ particles excited by 980 nm and recorded at room temperature.

the samples doped with Ho and Yb noticeably differ from that of the undoped sample. This difference is negligible in the spectral region where a lower-energy part of Raman spectrum of undoped $CaGd_2(MoO_4)_4$ is found, while the spectral region of a higher-energy part of the Raman spectra is strongly modified. At the same time, the shapes of the spectra of all Ho,Yb-containing samples are very similar to each other and weakly vary with the dopants' content. The wavelength region of a higher-energy part of the Raman spectra fairly coincides with the UC luminescence observed for codoped samples using the excitation at 980 nm, as well as with the well-known holmium luminescence in many other hosts (see, e.g. Ref. [60]). Thus, it can be concluded that the spectra shown in the right part of Fig. 12 are not Raman and relate to emission due to electron transitions at Ho^{3+} levels. This conclusion is supported by Fig. 9S presenting the difference spectra between codoped and

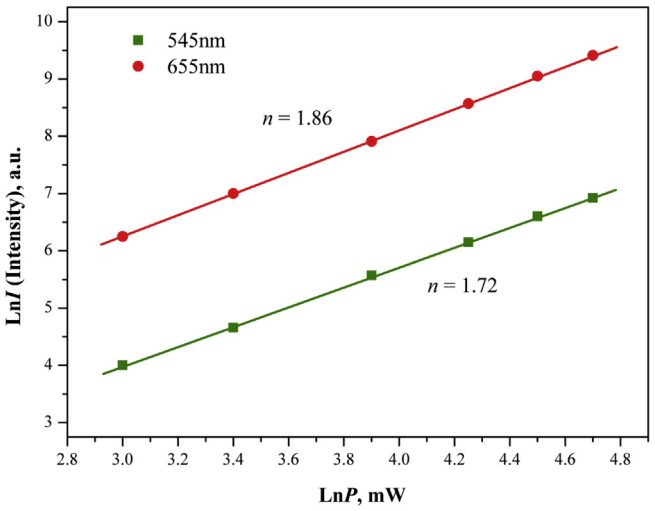

Fig. 9. The logarithmic scale dependence of the upconversion emission intensity on the pump power in the range from 20 to 110 mW at 545 and 655 nm in the $CaGd_{2-x}(MoO_4)_4$:yYb,zHo system.

undoped $CaGd_2(MoO_4)_4$ samples in comparison with the $HoAl_3(BO_3)_4$ luminescence spectrum from Ref. [60]. Compliance of the spectral regions occupied by difference spectra with the spectral region of Ho luminescence is evident, while a different shape of subbands is understandable with respect to a different local environment of Ho in $CaGd_2(MoO_4)_4$ (distorted square antiprism) and $HoAl_3(BO_3)_4$ (distorted trigonal prism). Another spectral feature can be deduced from a comparison of luminescence spectrum of the holmium ion taken at LabRam Aramis with the resolution 2 cm^{-1} (Fig. 12, wavelength region above 534 nm, and Fig. 9S) and the reference spectrum of $HoAl_3(BO_3)_4$ crystal. Evidently, while the reference spectrum clearly presents the result of splitting the excited and ground states by the crystal field as a number of intraband peaks, the luminescence band of Ho in the

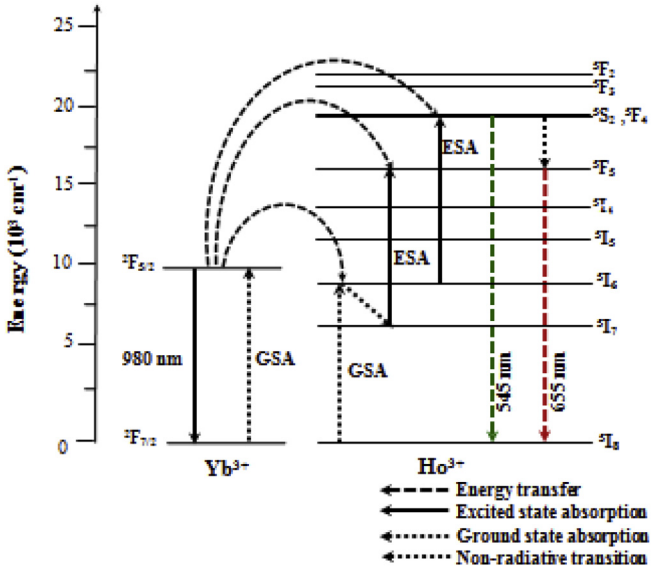

Fig. 10. The schematic energy level diagrams of Yb^{3+} (sensitizer) and Ho^{3+} ions (activator) ions in the $CaGd_{2-x}(MoO_4)_4$:yYb,zHo system and the upconversion mechanisms of the green and red emissions under 980 nm laser excitation. (For interpretation of the references to colour in this figure legend, the reader is referred to the web version of this article.)

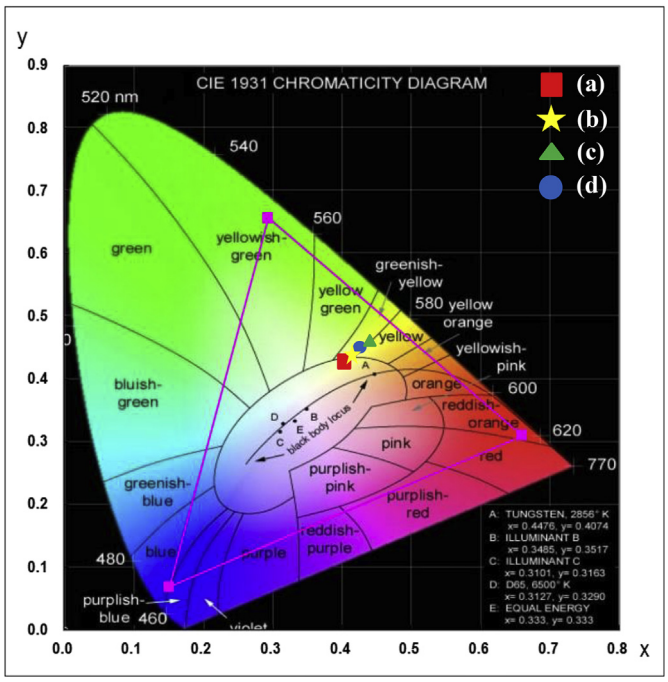

Fig. 11. The CIE chromaticity diagram showing the color coordinates of the $CaGd_{2-x}(MoO_4)_4$:*y*Yb,*z*Ho phosphors. The yellow emission for samples (a) $CaGd_{1.6}(MoO_4)_4$:$Yb_{0.35}$/$Ho_{0.05}$, (b) $CaGd_{1.55}(MoO_4)_4$:$Yb_{0.40}$/$Ho_{0.05}$, (c) $CaGd_{1.5}(MoO_4)_4$:$Yb_{0.45}$/$Ho_{0.05}$, and (d) $CaGd_{1.55}(MoO_4)_4$:$Yb_{0.50}Ho_{0.05}$ is shown in the insert. (For interpretation of the references to colour in this figure legend, the reader is referred to the web version of this article.)

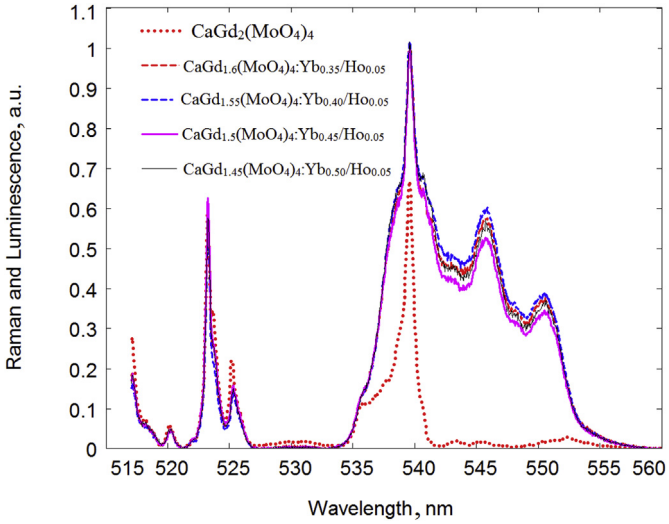

Fig. 12. The emission spectra of undoped $CaGd_2(MoO_4)_4$ (dotted) and Ho,Yb-codoped $CaGd_2(MoO_4)_4$. The undoped $CaGd_2(MoO_4)_4$ emission is predominantly due to Raman contribution (see also Fig. 7). The doped $CaGd_2(MoO_4)_4$ emission has the Ho luminescence contribution above 534 nm.

$CaGd_{2-x}(MoO_4)_4$:Yb_y/Ho_z lattice exhibits a strong broadening that almost completely washes out the interband substructure. This broadening is the result of a statistical disorder of Ho local environment inside the $CaGd_{2-x}Yb_y(MoO_4)_4$ lattice.

4. Conclusions

In the present study, the $CaGd_2(MoO_4)_4$:Ho^{3+}/Yb^{3+} phosphors with the doping concentrations of Ho^{3+} and Yb^{3+} ($x = Ho^{3+} + Yb^{3+}$, $Ho^{3+} = 0$ and 0.05, and $Yb^{3+} = 0$, 0.35, 0.40, 0.45 and 0.50) have been successfully synthesized by the microwave sol-gel method, and the structural and upconversion photoluminescence properties have been investigated. The synthesized particles, being formed after heat-treatment at 900 °C for 16 h, showed a well crystallized morphology. All compounds are (3 + 2)D incommensurately modulated with superspace group $I4_1/a(\alpha,\beta,0)00(-\beta,\alpha,0)00$ which is consistent with all the previously studied tetragonal molybdates $MRE_2(MoO_4)_4$. It was found that the $(\alpha^2 + \beta^2)^{1/2}$ parameter linearly increases with an increasing cell parameter *a* for all studied compounds and, therefore, modulation vector ***k*** is the same for all $CaRE_2(MoO_4)_4$ compounds. The modulation vector invariance is a specific and valuable feature of this structural type and the distance-dependent Coulomb interaction seems to be the source of the ordered vacancy/cation distribution. It could be reasonably supposed that similar behavior of the $(\alpha^2 + \beta^2)^{1/2}$ parameter may be found in other $MRE_2(MoO_4)_4$ and $MRE_2(WO_4)_4$ crystals.

Under the excitation at 980 nm, the particles doped with upconverting ions exhibited excellent yellow emissions based on a strong 545-nm emission band in the green region and a very strong 655-nm emission band in the red region. The pump power dependence and Commission Internationale de L'Eclairage chromaticity of the UC emission were evaluated. The shape of UC bands in CGM is found to be dependent on the Yb ion content due to the influence of the crystal field affecting the holmium ion. Thirteen Raman-active modes of the $CaGd_2(MoO_4)_4$ lattice were identified via a comparison of the experimental Raman spectra and the results of lattice dynamics simulations. Four additional Raman lines were found in the region of stretching vibrations, while at least two additional modes are present in the bending mode region. These additional modes are ascribed to the incommensurate modulation of crystal lattice, while no effect of incommensurate modulation on luminescence was detected. The luminescence bands of Ho ions are severely broadened due to a statistical disorder of Yb and Gd ions in the $CaGd_{2-x}Yb_y(MoO_4)_4$ lattice.

Acknowledgements

This research was supported by the Basic Science Research Program through the National Research Foundation of Korea funded by the Ministry of Education (2015-058813) and the Russian Foundation for Basic Research (15-52-53080). VVA, ASA and ASO were partially supported by the Ministry of Education and Science of the Russian Federation.

Appendix A. Supplementary data

Supplementary data related to this article can be found at http://dx.doi.org/10.1016/j.jallcom.2016.06.134.

References

[1] Henning A. Höppe, Recent developments in the field of inorganic phosphors, Angew. Chem. Int. Ed. 48 (2009) 3572–3582.
[2] Qiang Zhang, Cai-Feng Wang, Lu-Ting Ling, Chen Su, Fluorescent nanomaterial-derived white light-emitting diodes: what's going on, J. Mater. Chem. C 2 (2014) 4358–4373.
[3] A.S. Aleksandrovsky, A.V. Malakhovskii, V.N. Zabluda, A.I. Zaitsev, A.V. Zamkov, Optical and magneto-optical spectra of europium-doped strontium tetraborate single crystals, J. Phys. Chem. Solids 67 (2006) 1908–1912.
[4] J.M. Ngaruiya, S. Nieuwoudt, O.M. Ntwaeaborwa, J.J. Terblans, H.C. Swart, Resolution of Eu^{2+} asymmetrical emission peak od $SrAl_2O_4$:Eu^{2+},Dy^{3+} phosphor by cathodoluminescence measurements, Mater. Lett. 62 (17–18) (2008) 3192–3194.
[5] Zhiguo Xia, Yuanyuan Zhang, Maxim S. Molokeev, Victor V. Atuchin, Structural and luminescence properties of yellow-emitting $NaScSi_2O_6$:Eu^{2+} phosphors: Eu^{2+} site preference analysis and generation of red emission by codoping

Mn^{2+} for white-light-emitting diode applications, J. Phys. Chem. C 117 (2013) 20847–20854.
[6] Chang Sung Lim, Synthesis of $BaMoO_4:Er^{3+}/Yb^{3+}$ particles by an MAM method and their upconversion photoluminescence properties, Mater. Chem. Phys. 140 (1) (2013) 154–158.
[7] Lan Ma, Zhiguo Xia, Victor Atuchin, Maxim Molokeev, S. Auluck, A.H. Reshak, Quanlin Liu, Engineering oxygen vacancies towards self-activated $BaLuAl_xZn_{4-x}O_{7-(1-x)/2}$ photoluminescent materials: an experimental and theoretical analysis, Phys. Chem. Chem. Phys. 17 (2015) 31188–31194.
[8] V.V. Atuchin, N.F. Beisel, E.N. Galashov, E.M. Mandrik, M.S. Molokeev, A.P. Yelisseyev, A.A. Yusuf, Zhiguo Xia, Pressure-stimulated synthesis and luminescence properties of microcrystalline $(Lu,Y)_3Al_5O_{12}:Ce^{3+}$ garnet phosphors, ACS Appl. Mater. Interfaces 7 (47) (2015) 26235–26243.
[9] Haipeng Ji, Zhaohui Huang, Zhiguo Xia, Yao Xie, Maxim S. Molokeev, Victor V. Atuchin, Facile solution-precipitation assisted synthesis and luminescence property of greenish-yellow emitting $Ca_6Ba(PO_4)_4O$: Eu^{2+} phosphor, Mater. Res. Bull. 75 (2016) 233–238.
[10] J.F. Suyver, A. Aebischer, D. Biner, P. Gerner, J. Grimm, S. Heer, K.W. Krämer, C. Reinhard, H.U. Güdel, Novel materials doped with trivalent lantanides and transition metal ions showing near-infrared to visible photon upconversion, Opt. Mater. 27 (6) (2005) 1111–1130.
[11] M. Haase, H. Schäfer, Upconverting nanoparticles, Angew. Chem. Int. Ed. 50 (2011) 5808–5829.
[12] Zhiguo Xia, Haiyan Du, Hayue Sun, NIR-to-blue, green, orange and white upconversion luminescence in $Yb^{3+}/Tm^{3+}/Er^{3+}/Ho^{3+}$-doped $Na_{0.5}Gd_{0.5}WO_4$ nanocrystals, J. Optoelect. Adv. Mater. 12 (5) (2010) 975–979.
[13] Takaaki Taniguchi, Tomoaki Murakami, Asami Funatsu, Kazuto Hatakeyama, Michio Koinuma, Yasumichi Matsumoto, Reversibly tunable upconversion luminescence by host–guest chemistry, Inorg. Chem. 53 (2014) 9151–9155.
[14] B.P. Singh, A.K. Parchur, R.S. Ningthoujam, P.V. Ramakrishna, S. Singh, P. Singh, S.B. Rai, R. Maalej, Enhanced up-conversion and temperature-sensing behaviour of Er^{3+} and Yb^{3+} co-doped $Y_2Ti_2O_7$ by incorporation of Li^+ ions, Phys. Chem. Chem. Phys. 16 (2014) 22665–22676.
[15] V. Loipur, G. Nikolic, M.D. Dramicanin, Luminescence thermometry below room temperature via up-conversion emission of $Y_2O_3:Yb^{3+}$, Er^{3+} nanophosphors, J. Appl. Phys. 115 (20) (2014) 203106.
[16] Chang Sung Lim, Aleksandr Aleksandrovsky, Maxim Molokeev, Aleksandr Oreshonkov, Victor Atuchin, Microwave sol-gel synthesis and upconversion photoluminescence properties of $CaGd_2(WO_4)_4:Er^{3+}/Yb^{3+}$ phosphors with incommensurately modulated structure, J. Solid State Chem. 228 (2015) 160–166.
[17] Shanshan Du, Deyin Wang, Yuhua Wang, Shuangyu Xin, QinPing Qiang, Xinlong Ma, Synthesis and up-conversion luminescence of $Yb^{3+}/Er^{3+}/Tm^{3+}$ doped $Ca_9Y(PO_4)_7$, New J. Chem. 39 (2015) 5605–5611.
[18] Chang Sung Lim, Aleksandr Aleksandrovsky, Maxim Molokeev, Aleksandr Oreshonkov, Victor Atuchin, The modulated structure and frequency upconversion properties of $CaLa_2(MoO_4)_4:Ho^{3+}/Yb^{3+}$ phosphors prepared by microwave synthesis, Phys. Chem. Chem. Phys. 17 (2015) 19278–19287.
[19] Dong He, Chongfeng Guo, Sha Jiang, Niumiao Zhang, Changkui Duan, Min Yin, Ting Li, Optical temperature sensing properties of Yb^{3+}–Er^{3+} co-doped $NaLnTiO_4$ (Ln : Gd, Y) up-conversion phosphors, RSC Adv. 5 (2015) 1385–1390.
[20] Chang Sung Lim, Microwave sol-gel process of $KGd(WO_4)_2:Ho^{3+}/Yb^{3+}$ phosphors and their upconversion photoluminescence properties, J. Phys. Chem. Solids 78 (2015) 65–69.
[21] A. Sedlmeier, D.E. Achatz, L.H. Fischer, H.H. Gorris, O.S. Wolfbeis, Photon upconversion nanoparticles for luminescent sensing of temperature, Nanoscale 4 (2012) 7090–7096.
[22] Weifeng Yang, Xiyan Li, Dongzhi Chi, Hongjie Zhang, Xiaogang Liu, Lanthanide-doped upconversion materials: emerging applications for photovoltaics and photocatalysis, Nanotechnology 25 (2014) 482001.
[23] Jaehong Key, James F. Leary, Nanoparticles for multimodal in vivo imaging in nanomedicine, Int. J. Nanomed 9 (2014) 711–726.
[24] Xiaoqing Hu, Jingxian Zhu, Xiyu Li, Xin Zhang, Qingyang Meng, Lan Yuan, Jiying Zhang, Xin Fu, Xiaoning Duan, Haifeng Chen, Yingfang Ao, Dextran-coated fluorapatite crystals doped with Yb^{3+}/Ho^{3+} for labeling and tracking chondrogenic differentiation of bone marrow mesenchymal stem cells in vitro and *in vivo*, Biomaterials 52 (2015) 441–451.
[25] Chang Sung Lim, Victor Atuchin, Aleksandr Aleksandrovsky, Maxim Molokeev, Aleksandr Oreshonkov, Microwave sol-gel synthesis of $CaGd_2(MoO_4)_4:Er^{3+}/Yb^{3+}$ phosphors and their upconversion photoluminescence properties, J. Am. Ceram. Soc. 98 (10) (2015) 3223–3230.
[26] Md Masuqul Haque, Dong-Kuk Kim, Luminescent properties of Eu^{3+} activated $MLa_2(MoO_4)_4$ based (M = Ba, Sr, Ca) novel red-emitting phosphors, Mater. Lett. 63 (2009) 793–796.
[27] Chongfeng Guo, Hyun Kyoung Yang, Jung-Hyun Jeong, Preparation and luminescent properties of phosphor $MGd_2(MoO_4)_4:Eu^{3+}$ (M = Ca, Sr, Ba), J. Lumin 130 (2010) 1390–1393.
[28] Ying-Chien Fang, Sheng-Yuan Chu, Po-Ching Kao, You-Ming Chuang, Zong-Liang Zeng, Energy transfer and thermal quenching behaviors of $CaLa_2(MoO_4)_4:Sm^{3+}$, Eu^{3+} red phosphors, J. Electrochem. Soc. 158 (2) (2011) J1–J5.
[29] Lin Qin, Yanlin Huang, Taiju Tsuboi, Hyo Jin Seo, The red-emitting phosphors of Eu3+-activated $MR_2(MoO_4)_4$ (M = Ba, Sr, Ca; R = La^{3+}, Gd^{3+}, Y^{3+}) for light emitting diodes, Mater. Res. Bull. 47 (2012) 4498–4502.
[30] V.A. Morozov, A. Bertha, K.W. Meert, S. Van Rompaey, D. Batuk, G.T. Martinez, S. Van Aert, P.F. Smet, M.V. Raskina, D. Poelman, A.M. Abakumov, J. Hadermann, Incommensurate modulation and luminescence in the $CaGd_{2(1-x)}Eu_{2x}(MoO_4)_{4(1-y)}(WO_4)_{4y}$ ($0 \le x \le 1$, $0 \le y \le 1$) red phosphors, Chem. Mater. 25 (2013) 4387–4395.
[31] Chang Sung Lim, Preparation of $SrGd_2(MoO_4)_4:Er^{3+}/Yb^{3+}$ phosphors by the microwave-modified sol-gel method and their upconversion photoluminescence properties, J. Korean Ceram. Soc. 51 (6) (2014) 605–611.
[32] Chang Sung Lim, Upconversion photoluminescence properties of $SrY_2(MoO_4)_4:Er^{3+}/Yb^{3+}$ phosphors synthesized by a cyclic microwave-modified sol-gel method, Inf. Phys. Technol. 67 (2014) 371–376.
[33] Artem M. Abakumov, Vladimir A. Morozov, Alexander A. Tsirlin, Johan Verbeeck, Joke Hadermann, Cation ordering and flexibility of the BO_4^{2-} tetrahedra in incommensurately modulated $CaEu_2(BO_4)_4$ (B = Mo, W) scheelites, Inorg. Chem. 53 (2014) 9407–9415.
[34] V.V. Atuchin, O.D. Chimitova, T.A. Gavrilova, M.S. Molokeev, Sung-Jin Kim, N.S. Surovtsev, B.G. Bazarov, Synthesis, structural and vibrational properties of microcrystalline $RbNd(MoO_4)_2$, J. Cryst. Growth 318 (2011) 683–686.
[35] V.V. Atuchin, V.G. Grossman, S.V. Adichtchev, N.V. Surovtsev, T.A. Gavrilova, B.G. Bazarov, Structural and vibrational properties of microcrystalline $TlM(MoO_4)_2$ (M = Nd, Pr) molybdates, Opt. Mater. 34 (2012) 812–816.
[36] Pinglu Shi, Zhiguo Xia, Maxim S. Molokeev, Victor V. Atuchin, Crystal chemistry and luminescence properties of red-emitting $CsGd_{1-x}Eu_x(MoO_4)_2$ solid-solution phosphors, Dalton Trans. 43 (2014) 9669–9676.
[37] V.V. Atuchin, A.S. Aleksandrovsky, O.D. Chimitova, T.A. Gavrilova, A.S. Krylov, M.S. Molokeev, A.S. Oreshonkov, B.G. Bazarov, J.G. Bazarova, Synthesis and spectroscopic properties of monoclinic α-$Eu_2(MoO_4)_3$, J. Phys. Chem. C 118 (28) (2014) 15404–15411.
[38] Y.L. Yang, X.M. Li, W.L. Feng, W.L. Li, C.Y. Tao, Co-precipitation synthesis and photoluminescence properties of (Ca1−x−y,Lny)MoO4: xEu3+ (Ln = Y, Gd) red phosphors J, Alloys Compd. 505 (2010) 239–242.
[39] V.V. Atuchin, O.P. Andreeva, I.V. Korolkov, E.A. Maximovskiy, C.S. Lim, Low-temperature synthesis and structural properties of $PbMoO_4$ nanocrystals, Asian J. Chem. 26 (5) (2014) 1287–1289.
[40] V.V. Atuchin, O.P. Andreeva, T.A. Gavrilova, N.A. Kalyzhnyi, I.V. Korolkov, E.A. Maximovskiy, Synthesis of mesoporous $CaMoO_4$ in aqueous solution, Solid State Phenom. 245 (2016) 80–85.
[41] Y. Huang, L. Zhou, Z. Tang, Self-assembled 3D flower-like NaY(MoO4)2:Eu3+ microarchitectures: hydrothermal synthesis, formation mechanism and luminescence properties, Opt. Mater. 33 (2011) 777–782.
[42] Y. Tian, B. Chen, B. Tian, J. Sun, X. Li, J. Zhang, L. Cheng, H. Zhong, H. Zhong, Q. Meng, R. Hua, Ionic liquid-assisted hydrothermal synthesis of dendrite-like NaY(MoO4)2:Tb3+ phosphor, Phys. B 407 (2012) 2556–2559.
[43] Z. Wang, H. Liang, L. Zhou, J. Wang, M. Gong, Q. Su, NaEu0.96Sm0.04(MoO4)2 as a promising red-emitting phosphor for LED solid-state lighting prepared by the Pechini process, J. Lumin 128 (2008) 147–154.
[44] Q. Chen, L. Qin, Z. Feng, R. Ge, X. Zhao, H. Xu, Upconversion luminescence of $KGd(MoO_4)_2:Er^{3+}$,Yb^{3+} powder prepared by Pechini method, J. Rare Earths 29 (2011) 843–848.
[45] Jeong Ho Ryu, Sang-Mo Koo, Jong-Won Yoon, Chang Sung Lim, Kwang Bo Shim, Synthesis of nanocrystalline $MMoO_4$ (M = Ni, Zn) phosphors via a citrate complex route assisted by microwave irradiation and their photoluminescence, Mater. Lett. 60 (13–14) (2006) 1702–1705.
[46] J. Zhang, X. Wang, X. Zhang, X. Zhao, X. Liu, L. Peng, Microwave synthesis of $NaLa(MoO_4)_2$ microcrystals and their near-infrared luminescent properties with lanthanide ion doping (Er^{3+}, Nd^{3+}, Yb^{3+}), Inorg. Chem. Commun. 14 (2011) 1723–1727.
[47] Chang Sung Lim, Microwave-assisted synthesis and photoluminescence of $MMoO_4$ (M = Ca, Ba) particles via a metathetic reaction, J. Lumin. 132 (7) (2012) 1774–1780.
[48] V. Petrícek, M. Dusek, L. Palatinus, Crystallographic computing system JANA2006: general features, Z. Krist. 229 (5) (2014) 345–352.
[49] W. Van Aalst, J. den Holander, W.J.A.M. Peterse, P.M. De Wolff, The modulated structure of γ-Na_2CO_3 in a harmonic approximation, Acta Cryst. B 32 (1) (1976) 47–58.
[50] T. Wagner, A. Schoenleber, A non-mathematical introduction to the superspace description of modulated structures, Acta Cryst. B 65 (3) (2009) 249–268.
[51] Chang Sung Lim, Highly modulated structure and upconversion photoluminescence properties of $PbGd_2(MoO_4)_4:Er^{3+}/Yb^{3+}$ phosphors, Mater. Res. Bull. 75 (2016) 211–216.
[52] A.X.S. Bruker, TOPAS V4: General Profile and Structure Analysis Software for Powder Diffraction Data. – User's Manual, Bruker AXS, Karlsruhe, Germany, 2008.
[53] V.V. Atuchin, T.A. Gavrilova, J.-C. Grivel, V.G. Kesler, Electronic structure of layered ferroelectric high-k titanate $La_2Ti_2O_7$, J. Phys. D. Appl. Phys. 42 (2009) 035305.
[54] V.V. Atuchin, B.G. Bazarov, T.A. Gavrilova, V.G. Grossman, M.S. Molokeev, Zh.G. Bazarova, Preparation and structural properties of nonlinear optical borates $K_{2(1-x)}Rb_{2x}Al_2B_2O_7$, $0 < x < 0.75$, J. Alloys Compd. 515 (2012) 119–122.
[55] P.G. Zverev, Vibronic relaxation of Raman modes in $CaMoO_4$ and $PbMoO_4$ molecular ionic crystals, Phys. Stat. Sol. C. 1 (11) (2004) 3101–3105.
[56] E. Sarantopoulou, C. Raptis, S. Ves, D. Christofilos, G.A. Kourouklis, Temperature and pressure dependence of Raman-active phonons of $CaMoO_4$: an

anharmonicity study, J. Phys. Condens. Matter 14 (39) (2002) 8925–8938.
[57] A.P.A. Marques, F.V. Motta, E.R. Leite, P.S. Pizani, J.A. Varela, E. Longo, D.M.A. de Melo, Evolution of photoluminescence as a function of the structural order or disorder in $CaMoO_4$ nanopowders, J. Appl. Phys. 104 (4) (2008) 043505.
[58] Hai-Hong Xi, Di Zhou, Hui-Dong Xie, Bin He, Qiu-Ping Wang, Raman spectra, infrared spectra, and microwave dielectric properties of low-temperature firing $[(Li_{0.5}Ln_{0.5})_{1-x}Ca_x]MoO_4$ (Ln = Sm and Nd) solid solution ceramics with scheelite structure, J. Am. Ceram. Soc. 98 (2) (2015) 587–593.
[59] M. Pollnau, D.R. Gamelin, S.R. Lüthi, H.U. Güdel, M.P. Hehlen, Power dependence of upconversion luminescence in lanthanide and trasition-metal-ion systems, Phys. Rev. B 61 (5) (2000) 3337–3346.
[60] D.A. Ikonnikov, A.V. Malakhovskii, A.L. Sukhachev, V.L. Temerov, A.S. Krylov, A.F. Bovina, A.S. Aleksandrovsky, Spectroscopic properties of $HoAl_3(BO_3)_4$ single crystal, Opt. Mater. 37 (2014) 257–261.